

A Strong-Strong Simulation on the Beam-Beam Effect in a Linac/Ring B Factory*

Rui Li and Joseph J. Bisognano
CEBAF, 12000 Jefferson Ave., Newport News, VA 23606

Abstract

Since the inherently low emittance required by the linac/ring B Factory implies high disruption for the linac bunch, previous investigations of the beam-beam tune shift limit may not apply. A strong-strong simulation scheme was developed based on a macroparticle model to simulate beam-beam interaction in this situation self-consistently. Included in the ring dynamics are linear betatron oscillations and synchrotron motion, as well as transverse and longitudinal damping and quantum excitation. As a benchmarking test, the coherent quadrupole effect in a ring/ring collider was observed by the simulation. The code was then used to study the stability of the storage ring bunch in a linac/ring collider, and yielded strong synchro-betatron coupling due to the deep envelope modulation of the linac bunch. It was, however, observed that when initial conditions for the linac beam were properly chosen to match the focusing provided by the ring beam at IP, the beam-beam tune shift limit of the ring beam can be comparable to that of a ring/ring collider.

1 Introduction

An asymmetric e^+e^- collider with 10 GeV center of mass energy can be used as a B Factory to study the CP violation in the B-meson system. The luminosity required for this purpose should have value of $\mathcal{L} > 10^{33} \text{ cm}^{-2}\text{s}^{-1}$, which is much higher than the currently observed luminosity on existing machines. For the collision of transversely Gaussian distributed e^+e^- bunches, the luminosity is given by

$$\mathcal{L} = \frac{N_+ N_- f_c}{2\pi \sqrt{\sigma_{x+}^2 + \sigma_{x-}^2} \sqrt{\sigma_{y+}^2 + \sigma_{y-}^2}}, \quad (1.1)$$

where N_{\pm} are the numbers of particles per bunch; f_c , the bunch collision frequency; and $\sigma_{x\pm}$ and $\sigma_{y\pm}$, the horizontal and vertical bunch sizes, respectively. The vertical beam-beam tune

*Work supported by U.S. D.O.E. contract #DE-AC05-84ER40150.

shift for the positron bunch, which characterizes the vertical focusing effect of the electron bunch on the approaching positron particles, is defined by

$$\xi_{y+} = \frac{r_0 N_- \beta_{y+}^*}{2\pi \gamma_+ \sigma_{y-} (\sigma_{x-} + \sigma_{y-})}, \quad (1.2)$$

where γ_+ and β_{y+}^* are the Lorentz factor and the vertical beta function at IP for the positron bunch, and r_0 , the classical electron radius. The other three beam-beam tune shift parameters can be obtained by the replacements $x \leftrightarrow y$ and/or $+ \leftrightarrow -$. According to Eq. (1.1), one needs to increase the collision frequency f_c and the charge intensities for both e^+ and e^- bunches in order to reach the goal of $\mathcal{L} = 10^{33-34} \text{ cm}^{-2}\text{s}^{-1}$. However, the intrinsic feature of nonlinearity in the beam-beam interaction sets a limit on the achievable beam-beam tune shift, which is typically around 0.06 for ring/ring colliders, above which the beam will start to blow up to a larger equilibrium bunch size in a few damping times. This beam-beam effect is primarily responsible for the limitation on the observed luminosity.

The idea of a linac/ring collider is proposed [1] such that the beam from the linac is not recycled after each collision. Typically, in these scenarios, the electron beam is provided by the linac and the harder-to-produce positron beam is accumulated in the storage ring. In the following, therefore, the linac particles are electrons; the storage ring particles, positrons. As a result, the charge intensity for the e^+ bunch is no longer restricted by the beam-beam tune shift limit for ξ_{y-} . It is expected that this will enlarge the parameter space available for the design of such a colliding scheme to accomplish the luminosity goal. An additional feature of a linac/ring B Factory is that at the required high luminosity, the relatively low average-beam-current capability of linacs compared to a storage ring implies low emittance. The consequently high positron charge density together with the low γ_- leads to high disruption for the electrons. The disruption parameter, D_{y-} , is defined as the ratio of the positron bunch length to the electron vertical focal length

$$D_{y-} = \frac{\sigma_{z+}}{f_{y-}} = \frac{2r_0 N_+ \sigma_{z+}}{\gamma_- \sigma_{y+} (\sigma_{x+} + \sigma_{y+})}. \quad (1.3)$$

For several given lists [2, 3] of design parameters, the parameter D_{y-} is of the order of 100, indicating that the electron particles oscillate through the positron bunch during each collision. The beam-beam dynamics experienced by the positron bunch is therefore disparate from that in a ring/ring collider, and the beam-beam tune shift limit for ξ_{y+} is not necessarily equal to the familiar number 0.06. Thus, to be confident of linac/ring B Factory performance estimates, one needs to study the stability of the positron beam in the storage ring when it undergoes collisions with highly disrupted electron bunches.

The simulation for the beam-beam effect in a linac/ring B Factory should be strong-strong since we are interested in the evolution of the strong (positron) beam in the process of its interaction with the relatively weak (electron) beam. In this study, a macro-particle model is employed to simulate the beam-beam interaction. This model was previously used [4] to display the high disruption effect on the electrons for a single collision of two round beams. Here an extended model is used to accommodate the interaction of elliptical beams. Care

has been taken in choosing the sizes of the macro-particles and the number of macro-particles necessary in each beam in order to obtain statistically reliable results. The dynamics of the storage ring beam is studied by tracking the macro-particles in the ring over a number of damping times, where each turn comprises the beam-beam interaction at the IR, the linear betatron oscillation, and the synchrotron motion, as well as the radiation damping and the quantum fluctuation effect.

In Sec. 2, we describe in detail the macro-particle model for the beam-beam interaction. Included in the appendix are also some analytical estimates of the effects of the sizes and the numbers of macro-particles used in the simulation on the calculations of the beam-beam forces and luminosities. As a benchmarking test, the simulation scheme was used to manifest the coherent quadrupole effect in ring/ring colliders for round beams. The reasonable agreement of our calculation with the existing results is shown in Sec. 3 [5, 6]. The beam-beam effect of a ring/ring collider using parameters given in the PEP B Factory proposal is studied in Sec. 4 [7, 8, 9]. We then proceed in Sec. 5 to investigate the behavior of the positron beam in a linac/ring B Factory. Strong synchro-betatron coupling in the motion of positron particles has been observed, which is induced by the pinches of the highly disrupted electron bunches during collisions. It is shown that the beam-beam limit for the parameter ξ_{y+} can be made comparable to that of a ring/ring collider when the electron bunches enter into the IR with properly matched [3] initial conditions. The effect of jitter in the linac beam is discussed in Sec. 6.

2 Simulation

In this section, the macro-particle model [10] used for the strong-strong beam-beam interaction is discussed. The overall layout of the program, including the simulation of the dynamics undergone by the bunches in the storage ring, is also presented.

2.1 Beam-Beam Interaction Model

At the IR of an e^+e^- collider, the two relativistic beams exert Lorentz forces on each other only in the transverse directions. The longitudinal motion of all the particles in a bunch is then uniform during a collision process. This allows us to divide each bunch longitudinally into many slices; the width of a slice corresponds to the longitudinal step size over which the charged particles are advanced in the collisions. Here, the number of slices should be sufficient to describe the beam-beam effect due to the longitudinal variation of the charge distributions. In the simulation, each slice is populated with macro-particles. The macro-particles in the two colliding beams experience mutual forces only when their corresponding slices overlap. Since the number of macro-particles is limited by computer capacity, shot noise often appears in the simulation results, and one needs to assign finite sizes to the macros to suppress this effect. This finite size macro-particle model does not impose any restriction on the charge distributions of the beams under study.

In the code, the force on each macro-particle is computed by direct Columb sum,

$$\mathbf{F}(\mathbf{r}_i^{(1)}) = \sum_m \mathbf{f}(\mathbf{r}_i^{(1)} - \mathbf{r}_m^{(2)}), \quad (2.4)$$

where $\mathbf{F}(\mathbf{r}_i^{(1)})$ is the total force on the i th macro in beam 1 at a given time step, and $\mathbf{f}(\mathbf{r}_i^{(1)} - \mathbf{r}_m^{(2)})$ is the force acting on the i th macro in beam 1 by the m th macro in beam 2 which lies in the same longitudinal interval as the former one. From the two-dimensional electrostatics, it has been shown [11] that the luminosity for each pair of interacting macros is related with their mutual force by

$$\mathcal{L}_{im} = \frac{\epsilon_0}{e^2} \nabla \cdot \mathbf{f}(\mathbf{b}), \quad (2.5)$$

where $\mathbf{b} = \mathbf{r}_i^{(1)} - \mathbf{r}_m^{(2)}$ is the displacement of the centers of the two macro-particles. The total luminosity can then be obtained by the sum over the luminosity for each interaction pair at each time step, namely

$$\mathcal{L} = \sum_{i,m} \mathcal{L}_{im}. \quad (2.6)$$

The aspect ratios for colliding beams in different designs vary in a wide range of values. For the general application of the simulation, the macro-particles are set to be Gaussian in charge distribution, with aspect ratio comparable to the designed beam aspect ratio. This will provide a better overlapping of macro-particles and hence reduce the spurious collisional effects (see Appendix A). Here, the electric fields on a two-dimensional grid, generated by a Gaussian macro-particle with given aspect ratio, are obtained from the well-known expression in terms of the complex error functions [12] and stored in a table. The mutual force for each interaction pair of macros is then readily calculated by interpolating data from the lookup table. This is actually not the force between two charge distributions, but rather the forces of one elliptic Gaussian macro-particle on a point charge, as if all the charge in the second macro-particle is at the center of the macro. More discussion on the simulation scheme can be found in Appendix A.

In certain situations, the sizes and the aspect ratio of the beam envelope evolve with time. This is particularly true in the linac/ring collision processes, where the electron bunches experience the pinching effect in each collision, and the positron bunches blow up in several damping times. Therefore, the modeling of the force generated by each slice of a bunch should be treated separately, with the sizes of the macros in each slice varied proportionally as the rms sizes of the corresponding slice evolve in each step of a collision. This will assure the proper description of the pinching effects. The ratio of the macro-particle size to the corresponding slice size is chosen to be $r = 0.5$ (see also Appendix A).

The finite macro-particle size plays the role of screening out the high-frequency shot noise effect in the force calculation. Nonetheless, due to the finite number of macro-particles in each slice, it is inevitable to have residual fluctuations of the distribution of macro-particles around the ideal physical distribution. In the case when the overall charge distribution for

a bunch in the storage ring changes slowly compared to the revolution period, the macro-particles in the bunch simulate different ensembles of the charge distribution in successive collisions due to their betatron motion in the ring. The average of the luminosities for these successive collisions then corresponds to the average over a certain number of ensembles and thus better simulates the true physical quantity. Reliable results should be insensitive to different random seeds, and their qualitative behavior should not change along with the increase of the number of macros used in the simulation.

In Fig. 1, the centers of 29 macro-particles are displayed, which simulate a Gaussian charge distribution with aspect ratio $R = 3.93$. The macro-particles have the same aspect ratio as the bunch but half the size. The total forces generated by these macro-particles are shown in Fig. 2 as the dotted curves, which are compared to the solid curves obtained analytically for the forces generated by a continuous Gaussian charge distribution. One can see that the high-frequency components of shot noise are suppressed by choosing finite sizes for the macros. However, this is accomplished at the cost of equivalently larger bunch sizes for the calculated forces, as described by Eq. (A.7). This effect explains the lower peak values for the calculated forces compared to the analytical results. Residual deviations for all the moments of distribution can also be seen in Fig. 2.

Comparison of simulation results using different number of macro-particles are shown in Fig. 3 and Fig. 4. In Fig. 3 we use $N_{m-} = 360$ macro-particles for the electron bunch and $N_{m+} = 1000$ macro-particles for the positron bunch. The electron bunch accelerated by a linac collides at IR with the positron bunch in the storage ring. The two bunches initially have the same transverse bunch sizes. After 3000 turns, the positron bunch blows up in the vertical direction as a result of beam-beam interaction. The equilibrium beam profiles right before the 3000th collision in the $Y - Z$ plane are shown in Fig. 3(a), and the dependence of the blowup factor on the number of revolutions of the positron bunch in the ring is shown in Fig. 3(b). The same calculation was carried out for $N_{m-} = 1440$ and $N_{m+} = 4000$. It turns out that the average equilibrium vertical bunch size in Fig. 3(b) agrees reasonably with that in Fig. 4(b), even though the result in the former plot has more fluctuations than that in the latter one—the expected consequence of a smaller number of macro-particles being used for the simulation. Reducing the sizes of macro-particles will require the increase of the number of macro-particles used for the simulation and thus also of the computer time consumed. Such tests have been done, yielding results quantitatively depending on the macro sizes according to Eq. (A.7). Such dependence is insensitive as long as Eq. (A.8) is satisfied.

2.2 Layout of the Program

To create a good picture of the beam dynamics, we start with the electron and positron bunches located at the pre-collision positions. The two bunches are then taken through each other and undergo the beam-beam interaction as described previously. In the case of the linac/ring colliding scheme, the electron bunches are dumped after each collision, and a new set of macro-particles with random Gaussian distribution is generated for each collision to

simulate the electron bunch newly accelerated from the linac. The beams in storage rings can be either both the electron and positron beams in a ring/ring collider, or only the positron beam in a linac/ring collider.

After each collision, the bunch in a storage ring is transported linearly from the post-collision position to the RF cavity, where the effect of transverse damping and quantum excitation is simulated once a turn [13]. Each macro-particle is then linearly transported from the RF cavity to the pre-collision position. During each turn, the longitudinal position for a macro-particle relative to the beam center is changed along with its energy [13], as a result of the synchrotron oscillation together with the longitudinal damping and diffusion.

To obtain the initial distribution of the macro-particles for a bunch in a storage ring, we start with setting all the macro-particles at the center point of the bunch. Being transported through all the dynamics in the ring for several damping times in the absence of beam-beam interaction, the macros eventually reach an equilibrium 3-D Gaussian distribution with specified nominal bunch sizes. Since no longitudinal motion is associated with the macro-particles for the electron bunch in the linac/ring collider, we distribute an equal number of macro-particles with transverse random Gaussian distribution to each slice in the bunch. The charges assigned to the macros in different slices of the linac bunch are scaled to the parabolic longitudinal charge distribution.

3 A Benchmarking Test

In Ref. [5], it is argued that the benchmarking of beam-beam simulation codes should use the physical phenomena predicted by theories and in the appropriate parametric regimes that have a clearly defined functional dependence. One of the proper candidates for this purpose of benchmarking is the coherent quadrupole beam-beam effect in ring/ring colliders. This phenomenon was predicted by Chao and Ruth [14] using a linearized Vlasov equation, and was first observed by Krishnagopal and Siemann in beam-beam simulation for the collision of round beams. It has the remarkable feature that at tunes just below the quarter-integer, the beam distributions oscillate in an anti-correlated manner with period 2.

With the observation of the beam distribution oscillation with period 2 as the criterion for our benchmark test, we use the parameters shown in Table 1 [5] for our simulation.

Here the two beams are round in the transverse plane and have no longitudinal length. The results of the functional dependence of the beam blowup factors and the luminosity vs. the number of revolutions are shown in Figs. 5(a) and 5(b). The anti-correlated oscillation of beam sizes with period 2 is clearly demonstrated in Fig. 5(c). Figure 6 shows the corresponding variation of the transverse beam distributions, where each beam oscillates between the two modes of being dense and hollow in the core. These results agree well with the previous results [5, 6, 15, 16] obtained using completely different simulation algorithms.

4 Results for the Ring/Ring Beam-Beam Effects

Another test of our code is the simulation of the beam-beam effect in the ring/ring B Factory. For this study we use the parameters in the PEP B Factory proposal [7], as shown in Table 2. The nominal luminosity is $\mathcal{L}_0 = 3 \times 10^{33} \text{ cm}^{-2}\text{s}^{-1}$, and the four nominal beam-beam tune shift parameters are all set to be $\xi_0 = 0.03$. Here each bunch, divided into five slices, is represented by 300 macro-particles. The macro-particles themselves are Gaussian charge distributions with sizes half of the nominal bunch sizes.

The beam-beam results in Ref. [7] are obtained at the working point $(\nu_x, \nu_y) = (0.9, 0.5)$ for both beams. However, at this working point, we observed a much bigger blowup for the e^+ beam than that shown in Ref. [7]. It is noticed that the parameters for the e^+ beam are close to the relation $\nu_s = \nu_x - \nu_y$. Hence, for the following simulation, the fractional tunes for both beams are selected at $(\nu_x, \nu_y) = (0.9, 0.6)$ to avoid the resonance.

In Fig. 7, we show the initial distribution of centers of the macros for the two colliding beams. The numbers of the macros in each slice are shown in Fig. 8. The dynamics for both beams is simulated over three damping times. The behavior of $\sigma_{y+,0}$ is shown in Fig. 9(a), and the behavior of the luminosity can be seen in Fig. 9(b). It turns out that as the result of beam-beam interaction, the bunch sizes increase in the first damping time and consequently cause the decrease of the luminosity. A set of equilibrium values can be reached for all the bunch sizes in a period of several damping times, from which the dynamical beam-beam tune shift parameters can be evaluated using Eq. (1.2).

The nominal beam-beam tune shift parameter ξ_0 can be changed by varying the charges in the two beams simultaneously. In Fig. 10 we show the equilibrium bunch sizes, luminosity and dynamical beam-beam tune shift parameters as functions of ξ_0 . One finds that the luminosity plot in Fig. 10(b) is quantitatively comparable with Fig. 4-88 in Ref. [7]. The saturation of the dynamical ξ_{y+} to a value of $\xi_{\text{lim}} \approx 0.04$ is shown in Fig. 10(c).

The significant phenomenon one observes is the blowup of the vertical size for the low-energy beam, which qualitatively agrees with the results in Ref. [7]. This limiting effect on the beam in the low-energy ring is unfavorable for further asymmetrization of the energies in the two rings.

5 Results for the Linac/Ring Beam-Beam Effects

We now focus our attention to the simulation of the beam-beam effect in the linac/ring B Factory. There have been several parameter lists proposed for the design of this colliding scheme [1, 2, 3]. The one shown in Table 3 is used here for our simulation. Notice that the proposed nominal luminosity is $\mathcal{L}_0 = 1 \times 10^{34} \text{ cm}^{-2}\text{s}^{-1}$, and the nominal beam-beam parameters are $\xi_{y+,0} = 0.056$ and $D_{y-,0} = 273.7$, indicating strong beam-beam interaction. Our goal is to study the beam-beam tune shift limit for the linac/ring collider, and to observe the dominant dynamics responsible for the beam-beam limitation. The simulation related parameters are listed in Table 4.

The profiles of the two beams in the $Y - Z$ plane before and after the first collision are shown in Fig. 11. For the e^- beam, the numbers of macro-particles are evenly distributed among the slices, with the longitudinal parabolic charge distribution characterized by the difference in the charges carried by macros in different slices. This is shown in Fig. 12(a). The longitudinal Gaussian charge distribution for the e^+ beam is simulated by the longitudinal Gaussian distribution of macros carrying the same amount of positive charges, as shown in Fig. 12(b). In the simulation, the e^+ beam is circulated in the storage ring, experiencing beam-beam collision at IP once a turn with a new electron bunch, and also undergoes the ring dynamics including the linear betatron oscillations, synchrotron oscillations, as well as the damping and diffusion in all three dimensions. The evolution of the positron vertical bunch size and the luminosity of beam-beam collision in about three damping times of the vertical motion is shown in Fig. 13, which demonstrates that the luminosity reaches an equilibrium value lower than the nominal one as the result of beam blowup.

To understand the cause of the beam blowup in the linac/ring beam-beam simulation, the trace of certain e^- macros and also the variation of rms for each e^- slice through the e^+ bunches during the first collision are plotted in Fig. 14. The formation of pinches when the e^- macros oscillate through the e^+ bunch is clearly seen as the effect of the high disruption of the e^- bunches (here $D_{ey} = 273.7$). It is expected that the consequent deep modulation of the e^- envelope in the collision processes will have a significant impact on the stability of the positron bunches by inducing (1) strong nonlinearity at the pinch points and (2) strong synchro-betatron coupling. This is believed to be the major mechanism for the observed beam blowup in Fig. 13(a).

To reduce the effect of pinches, a matching scheme was developed by S. Heifets [3]. By “matching” it is meant that the transverse bunch sizes for the e^- and e^+ bunches are set to be equal at IP, i.e., $\sigma_{x-,0}^* = \sigma_{x+,0}^*$ and $\sigma_{y-,0}^* = \sigma_{y+,0}^*$. This is achieved by determining the initial condition for the e^- bunch through tracking the matched e^- bunch at IP back to the beginning of the interaction region (IR). The pre-collision phase space distribution of the e^- macros thus properly chosen allows the spreading out of the focusing points and produces a much smoother envelope distribution for the e^- bunches, as shown in Fig. 15. Similar to Fig. 13, the long term behavior of the positron bunch size and the luminosity can also be obtained in the case of matching.

We then proceed to study the beam-beam effect for both matching and nonmatching cases by varying $\xi_{y+,0}$ while fixing $D_{y-,0}$. This is done by varying the total charge of the e^- beam N_- while fixing the total charge of the e^+ beam N_+ . The dependence of the equilibrium values of the beam blowup factor and luminosity with respect to different $\xi_{y+,0}$ is shown in Fig. 16. As shown in Fig. 16(a), for the non-matching case, the beam starts to blow up around $\xi_{y+,0} = 0.02$, whereas the blowup takes place around $\xi_{y+,0} = 0.05$ if matching applies. Also the extent of beam blowup as $\xi_{y+,0}$ increases for the non-matching case is much larger than the matching situation. In Fig. 16(b), the luminosities deviate from the nominal (no beam-beam interaction) behavior as the result of beam blowup (here the luminosity and the beam sizes do not straightforwardly satisfy Eq. (1.1) because of the focusing phenomena involved for the e^- macros). It is shown that, for $\xi_{y+,0}$ above the value of 0.06, the luminosity

in the matching case increases slowly with values larger than the saturated value in the non-matching cases. The above comparison of the beam-beam effect with and without matching manifests the effect of envelope modulation of the e^- bunches.

The results in Figs. 13 and 16 were obtained for the fractional betatron tune (Q_{x+}, Q_{y+}) being $(0.64, 0.54)$. As the further investigation of the beam-beam effect in linac/ring scenarios, we studied the dependence of the equilibrium beam blowup factor $\sigma_{y+}/\sigma_{y+,0}$ on the choice of (Q_{x+}, Q_{y+}) for the storage ring beam. Since the simulation is strong-strong and time consuming, the blowup is computed on sporadic points in the tune plane reasonably chosen in interesting areas instead of sweeping the grids in the tune plane. The following are the descriptions of the general behavior observed. First, for the low-disruption cases ($D_{y-,0} < 1$), one can see clearly the transverse resonance structure and the synchrotron sidebands in the tune plane. This is similar to the beam-beam interaction in the ring/ring collider, when the collisions of the two beams take place without the oscillation of the electrons or pinching of the electron beam. Secondly, when matching is applied to the high-disruption case ($D_{y-,0} = 273.3$), the transverse resonance structure can be observed as a strong localized enhancement of the low-level beam blowup in the tune plane. This indicates that when matching applies, apart from the residual modulation of the e^- envelope, the beam-beam limit is approximately caused by the same nonlinearity effect as in the ring/ring situation. Lastly, for the high-disruption case without matching, the general phenomenon one found is that when the modulation of σ_{y-} becomes deeper as $D_{y-,0}$ increases, the equilibrium bunch size σ_{y+} varies from the unperturbed value in most of the tune plane to the situation of overall blowup. This agrees with the results obtained by Gerasimov [17] using a weak-strong simulation with envelope-modulated electron bunches. It is also found that when the synchrotron motion of the e^+ beam is turned off in the simulation, the equilibrium beam blowup factor is much smaller compared to that obtained in the presence of the synchrotron motion. This implies that the overall beam blowup in the tune plane is mainly caused by the synchro-betatron coupling induced by the envelope modulation of the e^- beam.

It is important to ensure the numerical stability of the simulation results with respect to the simulation parameters. As shown in Figs. 3 and 4, the same equilibrium beam blowup value is obtained for different numbers of macros for the simulation. We also found that the results agree for different numbers of slices for the two beams (5 for the e^- bunch and 25 for the e^+ bunch as opposed to our previous parameters—9 for e^- bunch and 45 for the e^+ bunch). With all these checks, we conclude that the stability of the positron bunch is strongly affected by the pinching of the e^- bunch in the non-matching case; on the other hand, the beam-beam tune shift limit for the e^+ bunch can be made comparable with that in the ring/ring beam-beam interaction provided that proper initial condition is set for the e^- bunches. In practice, the hourglass effect for the e^- beam due to the strong focusing at IR often gives rise to a natural matching condition.

6 Effect of Jitters

Since the number of macros is limited in the simulation, a fluctuation of the transverse offset for each slice in the two beams is inevitable. These offsets are random and of the order $\sigma_{x,y}^{\text{slice}}/\sqrt{N_m^{\text{slice}}}$, where $\sigma_{x,y}^{\text{slice}}$ are the rms sizes of a given slice simulated by N_m^{slice} number of macro-particles. Without any treatment of these offsets in the simulation, the positron bunch shows a kink instability in the absence of synchrotron oscillations. It has been observed [18] that as the highly disrupted electron particles oscillate through the positron bunch, the effects of the offsets in the previous positron slices are passed to the later slices by the electrons. After many turns, the offsets in the positron slices are cumulatively enhanced in a coherent manner by this dipole interaction. Further simulation shows that the coherence in the dipole motion tends to be suppressed by synchrotron motion of the positron particles. The results of the beam-beam effect in a linac/ring collider presented in the previous section are obtained by removing the offset effects in the force calculation of the simulation, corresponding to ideal head-on collisions.

In reality, however, the e^- bunches from the linac could fluctuate in intensity, transverse position, longitudinal position (timing), and possibly shape. It is important to investigate the impact of these possible jitters of the linac beam on the stability of the storage ring beam. A complete description of the problem includes the coherent motion of the two beams, the effect of external colored noise on the nonlinear dynamical system, and the multi-dimensional couplings as well as the effect of damping and quantum diffusion.

In Ref. [19], the first-order effects of white noise jitters are estimated analytically by using a one-dimensional linear model. It shows that the required jitter tolerances are at the margin of the precision of measurements. Weak-strong simulations without damping [20] basically confirmed the above analytical prediction. As suggested in Ref. [20], the weak-strong simulation reveals the *initial* emittance growth of the e^+ beam. In a long term, the blowup of the e^+ beam will reduce the disruption of the e^- beam, and thus the effects of the pinches.

Here we studied the effect of the intensity jitter in order to reach an understanding consistent with previous predictions. First, a weak-strong simulation was carried out using an analytic beam-beam force formula for round beams, with the round positron beam represented by 500 particles. For the calculation, the damping times used were $\tau_x = \tau_y = 2.4$ ms, and the jitter of the electron current was 10%. The beam-beam tune shift parameters were set at $\xi_{x+,0} = \xi_{y+,0} = 0.055$, and the beams were assumed to have no longitudinal lengths. The fractional betatron tunes were chosen to avoid the linear weak-strong instability [21]. The destructive effect of intensity jitter, when the force is *linear*, is shown in Fig. 17(a). Figure 17(b) shows that the presence of damping can slow down the rate of beam blowup, but the beam is still far from stability. This is because the magnitude of the intensity jitter here is above the stability threshold predicted in Ref. [19] based on the linear model. However, when the *nonlinear* beam-beam force is used at IP, as shown in Fig. 18(a), the intensity jitter is much less destructive than that in a *linear* case. Furthermore, when transverse damping is applied to the *nonlinear* beam-beam interaction, the stability of the e^+ beam is restored,

as shown in Fig. 18(b) (the same result was obtained by C. D. Johnson [22]). The result in Fig. 18(a) is consistent with the results in Ref. [20], where the amplitude growth of positron particles is studied in a weak-strong simulation with synchrotron motion included. However, the effect of synchro-betatron coupling is small when studying particles with small synchrotron amplitudes [22].

We next studied the effect of jitters using our strong-strong beam-beam simulation, using the machine parameters in Table 3 and simulation parameters in Table 4. In the absence of the synchrotron motion, the same feature of the effect of damping in a nonlinear potential as shown in Fig. 18 is observed. We thus conclude that the internal jitter caused by the shot noise in the simulation plays a negligible role in the study of the effect of the external intensity jitter. With the inclusion of the synchrotron motion, however, the e^+ beam blows up even when the linac beam has no intensity jitters, as shown in Fig. 19(a). This is the result of the synchro-betatron coupling induced by the deep envelope modulation of the e^- beam. It is shown in Fig. 19(b) that the presence of jitter gives only 10% increase in the beam blowup compared to the case in Fig. 19(a). Moreover, when damping is applied, the effect of jitter can hardly be seen when we compare the result in Fig. 19(c) with that in Fig. 13(a). The latter is obtained in the absence of jitter.

In the above study, we used random white noise for the intensity jitter. In actual experiment, the power spectrum for the jitters of the linac beam depends on the characteristics of the photo cathode gun. For example, in a few-millisecond circulation time for the e^+ beam, 60 Hz noise acts as a constant offset; the e^+ beam would be more responsive to noise with frequencies in the kilohertz range. To study the effect of jitters of the linac beam for a specific design, it is important to know the power spectrum of the jitter and to take the complete dynamics for the e^+ beam into account.

7 Summary

In this study, a strong-strong beam-beam simulation is developed based on a macro-particle model. The motion of the macro-particles is 3-D, and the effects of damping and quantum diffusion in the storage ring are also included. The dependence of the computation results on the simulation parameters, such as the size and the number of the macros chosen, is also estimated. As a benchmarking test, this simulation reveals the same coherent quadrupole effect in the ring/ring collider as observed by others.

This simulation scheme is first applied to study the beam-beam effect in a ring/ring B Factory, using the parameters in the PEP B Factory proposal. The beam-beam results thus obtained agree qualitatively with the published results. Quantitative comparison of the results requires further knowledge of the details of the simulations involved. We then use our simulation to study the beam-beam effect in a linac/ring B Factory. For $D_{y-,0} = 273.7$, the e^+ beam starts to blow up in the vertical direction at $\xi_{y+,0} = 0.02$. On the other hand, if the pre-collision state of the e^- bunches is properly chosen to smooth out the pinches, the beam-beam tune shift limit for the e^+ beam is found to be around 0.05, which is comparable

with that value in a ring/ring B Factory.

The effect of intensity jitter in the linac beam on the stability of the storage ring beam is also tested using our strong-strong simulation. With the inclusion of all the possible dynamics in the simulation, the extremely unstable situation for the positron bunch predicted by the weak-strong simulation without damping and an analytic model based on the linear beam-beam interaction is not observed.

Acknowledgements

We have benefitted greatly from conversations with G. A. Krafft on the macro-particle model for the beam-beam interaction, and from the original code SWARM written by J. Boyce. The information provided by C. D. Johnson, S. Krishnagopal, and M. A. Furman is gratefully acknowledged. The discussion with H. Liu on the screening effect of the macro-particle model was also illuminating.

Appendix A

To estimate the effect of the finiteness of (1) the sizes of macro-particles and (2) the number of macros in each bunch on the results of the beam-beam interaction using the macro-particle model, we take the familiar *Gaussian* bunch distribution as an example.

First we study the effect of finite size of the macro-particles. Consider a system of macro-particles. Let $\rho_c(\mathbf{x}, t)$ denote the distribution function for the center of the macro-particles. And let $S(\mathbf{x})$ denote the charge distribution in each single macro-particle, which corresponds to its finite size. The overall charge distribution function of the system, $\rho(\mathbf{x}, t)$, is then [23]

$$\rho(\mathbf{x}, t) = \int d\mathbf{x}' S(\mathbf{x} - \mathbf{x}') \rho_c(\mathbf{x}', t). \quad (\text{A.1})$$

The Fourier transform of the above equation gives

$$\tilde{\rho}(\mathbf{k}, t) = \tilde{S}(\mathbf{k}) \tilde{\rho}_c(\mathbf{k}, t), \quad (\text{A.2})$$

where

$$\tilde{S}(\mathbf{k}) = \int d\mathbf{x} S(\mathbf{x}) e^{-i\mathbf{k}\mathbf{x}}, \quad (\text{A.3})$$

and $\tilde{\rho}_c(\mathbf{k}, t)$ and $\tilde{\rho}(\mathbf{k}, t)$ are transformed from $\rho_c(\mathbf{x}, t)$ and $\rho(\mathbf{x}, t)$ in a similar way, respectively.

Assume a slice of a charged beam is represented by N_m macro-particles. The centers of the macro-particles are subject to a *continuous* 2-D Gaussian distribution with the rms bunch sizes σ_{xB} and σ_{yB} , namely,

$$\rho_c(x, y) = \frac{N_m}{2\pi\sigma_{xB}\sigma_{yB}} e^{-\frac{x^2}{2\sigma_{xB}^2} - \frac{y^2}{2\sigma_{yB}^2}}, \quad \text{or} \quad \tilde{\rho}_c(k_x, k_y) = N_m e^{-\frac{k_x^2\sigma_{xB}^2}{2} - \frac{k_y^2\sigma_{yB}^2}{2}}. \quad (\text{A.4})$$

Let each macro-particle be a 2-D Gaussian charge distribution carrying a charge q_m , with rms sizes σ_{xm} and σ_{ym} ,

$$S(x, y) = \frac{q_m}{2\pi\sigma_{xm}\sigma_{ym}} e^{-\frac{x^2}{2\sigma_{xm}^2} - \frac{y^2}{2\sigma_{ym}^2}}, \quad \text{or} \quad \dot{S}(k_x, k_y) = q_m e^{-\frac{k_x^2 \sigma_{xm}^2}{2} - \frac{k_y^2 \sigma_{ym}^2}{2}}. \quad (\text{A.5})$$

As the result of Eq. (A.2), the system of macro-particles yields an overall Gaussian distribution, which satisfies

$$\dot{\rho}(k_x, k_y) = N_m q_m e^{-\frac{k_x^2 (\sigma_{xB}^{\text{eff}})^2}{2} - \frac{k_y^2 (\sigma_{yB}^{\text{eff}})^2}{2}}. \quad (\text{A.6})$$

Here σ_{xB}^{eff} and σ_{yB}^{eff} are the effective rms bunch sizes,

$$\sigma_{xB}^{\text{eff}} = \sqrt{\sigma_{xB}^2 + \sigma_{xm}^2} \quad \text{and} \quad \sigma_{yB}^{\text{eff}} = \sqrt{\sigma_{yB}^2 + \sigma_{ym}^2}. \quad (\text{A.7})$$

We thus conclude that a system of continuously Gaussian distributed macro-particles, with the inner charge distribution for each macro-particle being also Gaussian, is equivalent to a Gaussian distribution of point particles with the rms sizes given by Eq. (A.7). As a consequence, the force generated by a distribution of charged *macro-particles* deviates from that generated by the same distribution of *point* charges. As shown in Fig. 2, this deviation is most obvious at the standard deviation of the distribution. This is called the edge effect. Also the luminosity for two overlapping slices in two colliding beams, which are simulated by macro-particles, satisfies Eq. (1.1) with the bunch sizes replaced by the effective bunch sizes given by Eq. (A.7). If the sizes for the macro-particles are properly chosen to satisfy

$$(\sigma_{xm}/\sigma_{xB})^2 \ll 1 \quad \text{and} \quad (\sigma_{ym}/\sigma_{yB})^2 \ll 1, \quad (\text{A.8})$$

the effects of finite size of macro-particle on the bias of the calculated results are negligible.

Next we discuss the effect of the finiteness of the number of macro-particles. For a system of a finite number of macro-particles, $\rho_c(\mathbf{x}, t)$, the distribution function for the center of the macro-particles, will contain high-frequency components instead of behaving smoothly as in Eq. (A.4). Since each macro-particle is a Gaussian distribution given by Eq. (A.5), we have $\dot{S}(k_x, k_y) \ll 1$ for $k_x \gg 1/\sigma_{xm}$ and $k_y \gg 1/\sigma_{ym}$. As a result, the high-frequency component in the overall charge distribution $\rho(x, y)$ is suppressed according to Eq.(A.2). This is the screening effect of the finite size of the macro-particles. We define N_0 as

$$N_0 = \frac{\sigma_{xB}\sigma_{yB}}{\sigma_{xm}\sigma_{ym}}, \quad (\text{A.9})$$

which is the number of macro-particles required to cover the bunch without overlapping. It can be shown that under the conditions of Eq. (A.8), the relative fluctuation of the luminosity \mathcal{L} for the interaction of the bunch with other charge distributions is small when the number of macro-particles in the bunch satisfies $N_m/N_0 \gg 2$, namely [24],

$$\langle \Delta \mathcal{L}^2 \rangle / \langle \mathcal{L} \rangle^2 \ll 1 \quad \text{when} \quad N_m/N_0 \gg 2. \quad (\text{A.10})$$

Here the ratio N_m/N_0 characterizes the degree of overlapping of the macro-particles.

Given the number of macro-particles in each bunch, the collisional effect due to the discreteness of the distribution can be suppressed by assigning finite sizes to the macro-particles. However, it is inevitable to have a residual low frequency fluctuation in the overall charge distribution due to the finiteness of the number of macro-particles. In our simulations, since the number of macro-particles is limited strongly by the computer time, we choose the sizes of the macro-particles relatively large (for most of our computations, we choose $\sigma_{xm}/\sigma_{xB} = 0.5$ or $\sigma_{ym}/\sigma_{yB} = 0.5$; smaller macro-particle sizes were used occasionally for error estimation) in order to have a better screening from the collisional effect. As the rms sizes of each slice in a bunch are updated for each step of advance in a collision, the sizes of the macro-particles in the slice are varied accordingly.

It should be noted that the aspect ratio of the macro-particles $R_m = \sigma_{xm}/\sigma_{ym}$ is fixed through the lookup table for the beam-beam forces. On the other hand, for interactions involving the pinch or blowup of the beams, the aspect ratio for each slice of a bunch $R_B = \sigma_{Bx}/\sigma_{By}$ evolves with time. Special care should be taken to ensure that Eq. (A.8) is always satisfied. In the simulation, the size of the macro-particles was chosen to be proportional to the size of the corresponding slice in the bunch, with the proportionality parameter r ($r^2 \ll 1$). When $R_B < R_m$, we set $\sigma_{mx} = r\sigma_{Bx}$, which gives $\sigma_{my} = r(R_B/R_m)\sigma_{By}$. In contrast, when $R_B > R_m$, we set $\sigma_{my} = r\sigma_{By}$, which leads to $\sigma_{mx} = r(R_m/R_B)\sigma_{Bx}$.

A reasonable extension of the above results to the simulation of the interaction for beams with *general* charge distribution is that the size of the macro-particles should be small compared to the characteristic length of the overall charge distribution, and the number of macro-particles should be enough so that the macros overlap one another to cover the dense region of the distribution.

References

- [1] P. Grosse-Wiesmann, SLAC-PUB-4545, 1988.
- [2] J. Bisognano, et al., 1988 Linear Accelerator Conference, 1988.
- [3] S. A. Heifets, G. A. Krafft and M. Fripp, Nuclear Inst. & Methods in Phys. Research, A295, p.286, 1990.
- [4] J. R. Boyce, S. Heifets and G. A. Krafft, 1990 Linear Accelerator Conference, p.724, 1990.
- [5] S. Krishnagopal and R. H. Siemann, LBL-32581, 1992.
- [6] S. Krishnagopal, private communication, 1992.
- [7] An Asymmetric B Factory Based on PEP — Conceptual Design Report, SLAC-PUB-372, 1991.

- [8] Y. Chin, DESY 87-011, 1987.
- [9] M. A. Furman, private communication, 1991.
- [10] Private communication with G. A. Krafft, 1991. The macro-particle model used here was originally developed to study the beam-beam interaction for round beams by G. A. Krafft and J. S. Wurtele based on R. Sah's SMASH program. In the present simulation the model is generalized by using Gaussian macro-particles of any given aspect ratio to study the interaction of elliptical beams.
- [11] G. A. Krafft, CEBAF TN-92-032, 1992.
- [12] M. Bassetti and G. A. Erskine, CERN-ISR-TH/80-06, 1980.
- [13] S. Krishnagopal and R. H. Siemann, Cornell Internal Note, CBN/88-1, 1988.
- [14] A. W. Chao and R. D. Ruth, *Part. Accel.* 16, p.201, 1985.
- [15] S. Krishnagopal and R. H. Siemann, Cornell Internal Note, CBN/88-8, 1988; R. H. Siemann, CBN/89-2, 1989.
- [16] Ph.D. Thesis, S. Krishnagopal, 1991.
- [17] A. Gerasimov, CEBAF-TN-90-243, 1990.
- [18] R. Li, G. A. Krafft, J. J. Bisognano, 1992 Linear Accelerator Conference Proceedings, p.752, 1992.
- [19] Y. Baconnier, CERN PS/91-02(LP), 1991.
- [20] C. D. Johnson, Proceedings of 1991 IEEE Particle Accelerator Conference, p.254, 1991.
- [21] A. W. Chao, SLAC-PUB-3179, 1983.
- [22] C. D. Johnson, private communication, 1992.
- [23] C. K. Birdsall, et al., *Methods in Computational Physics*, 9, p.241, 1970.
- [24] A similar result for round macro-particles has been obtained previously by G. A. Krafft.

Table 3: Linac/Ring B Factory Parameter List

Linac(e ⁻)	Storage Ring(e ⁺)
$E_- = 3.5$ GeV	$E_+ = 8.0$ GeV
$N_- = 0.544 \times 10^9$	$N_+ = 6.1 \times 10^{11}$
$f_c = 20.0$ MHz	$n_B = 30$
$\epsilon_{x-,0} = 5.75$ nm	$\epsilon_{x+,0} = 5.75$ nm
$\epsilon_{y-,0} = 0.37$ nm	$\epsilon_{y+,0} = 0.057$ nm
$\beta_{x-,0}^* = 3.32$ mm	$\beta_{x+,0}^* = 3.33$ mm
$\beta_{y-,0}^* = 3.33$ mm	$\beta_{y+,0}^* = 21.55$ mm
$\sigma_{x-,0}^* = 4.37$ μ m	$\sigma_{x+,0}^* = 4.37$ μ m
$\sigma_{y-,0}^* = 1.11$ μ m	$\sigma_{x+,0}^* = 1.11$ μ m
$\sigma_{z-} = 2.64$ mm	$\sigma_{z+} = 3.3$ mm
$D_{x-,0} = 69.6$	$\nu_s = 0.07$
$D_{y-,0} = 273.7$	$\tau_x = 0.9$ msec
	$\tau_y = 2.4$ msec
	$\tau_\delta = 6.9$ msec
	$\xi_{x+,0} = 0.002$
	$\xi_{y+,0} = 0.056$
$\mathcal{L}_0 = 1.1 \times 10^{34}$ cm ⁻² sec ⁻¹	

Table 4: Parameters for Simulation

	e ⁻	e ⁺
Number of Slices	9	45
Number of Macros	360	1000
Aspect Ratio of Macros	3.93	
Sizes of Macros	0.5 \times beam sizes	

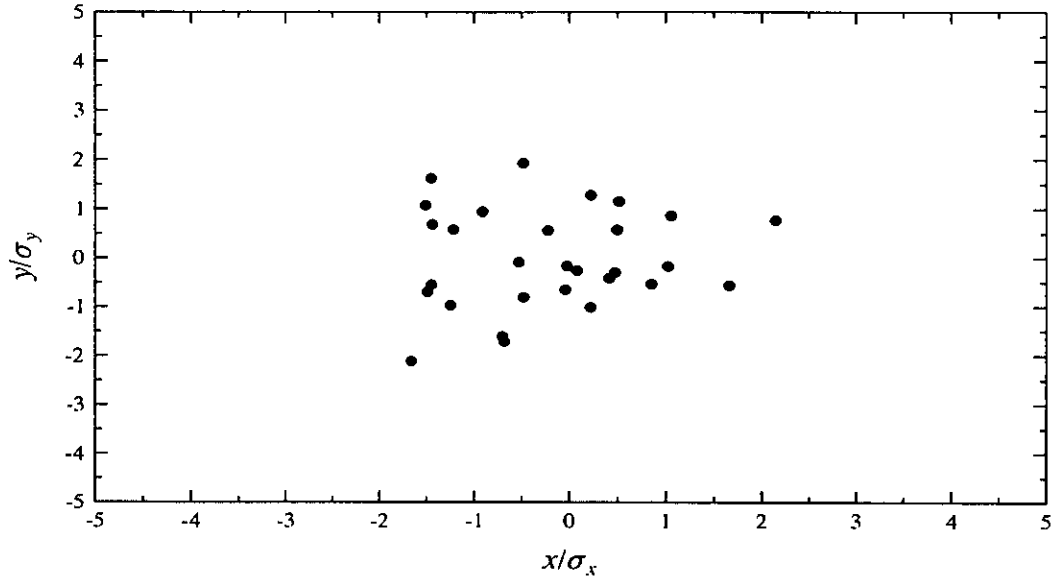


Figure 1: Transverse Gaussian distribution simulated by 29 macro-particles.

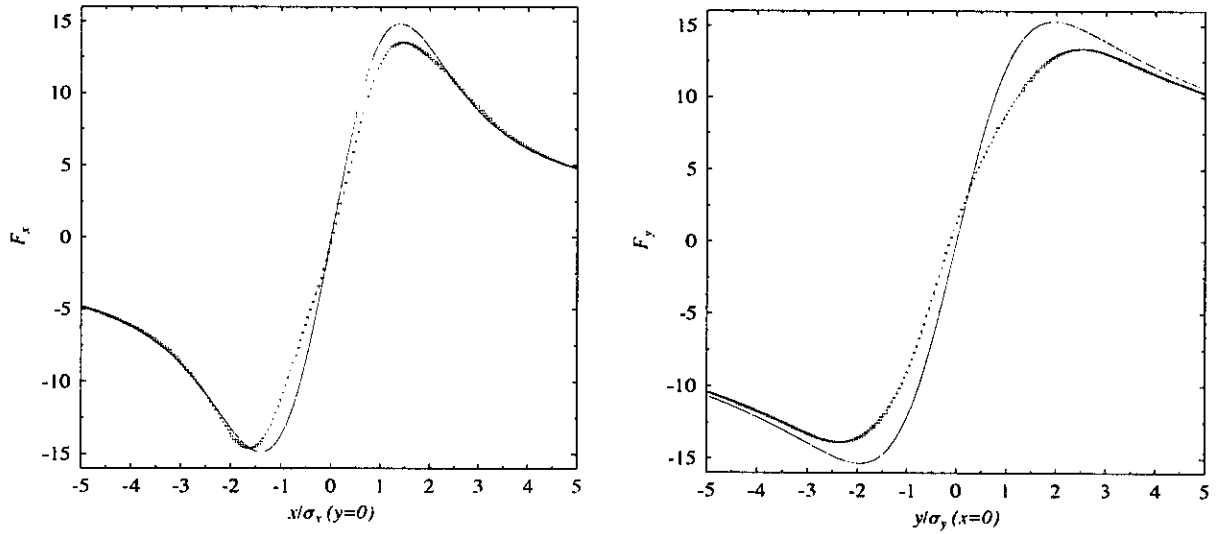


Figure 2: Force calculated by macro-particle model (dotted curves) compared to analytical results (solid curves) for the distribution in Fig. 1.

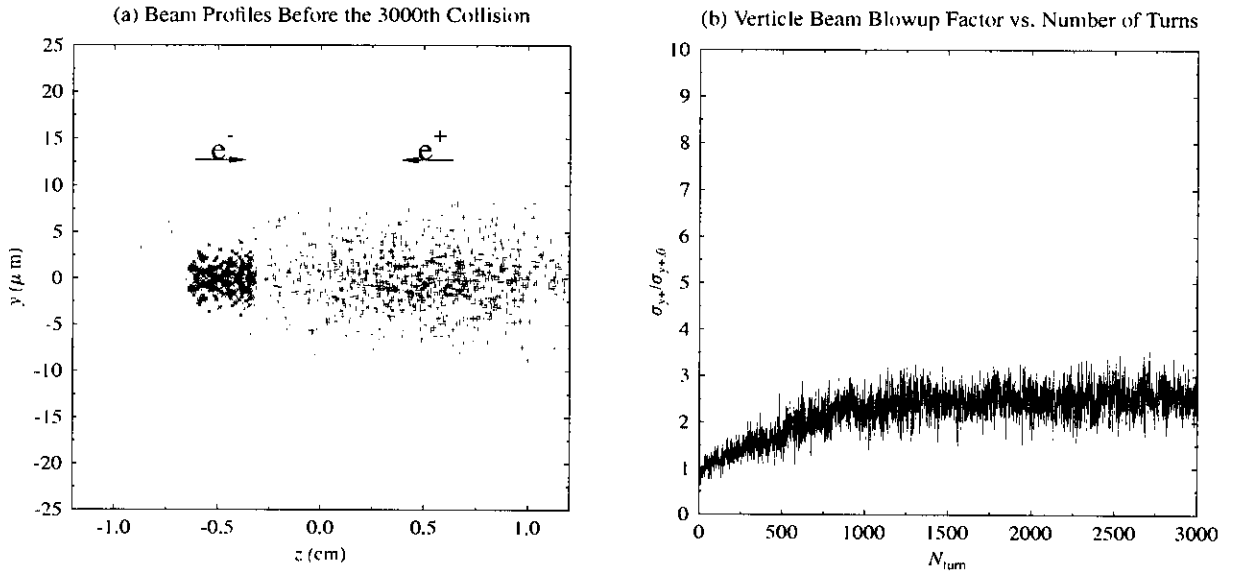


Figure 3: Simulation results using the number of macro-particles $N_{m-} = 360$ for the electron bunch and $N_{m+} = 1000$ for the positron bunch.

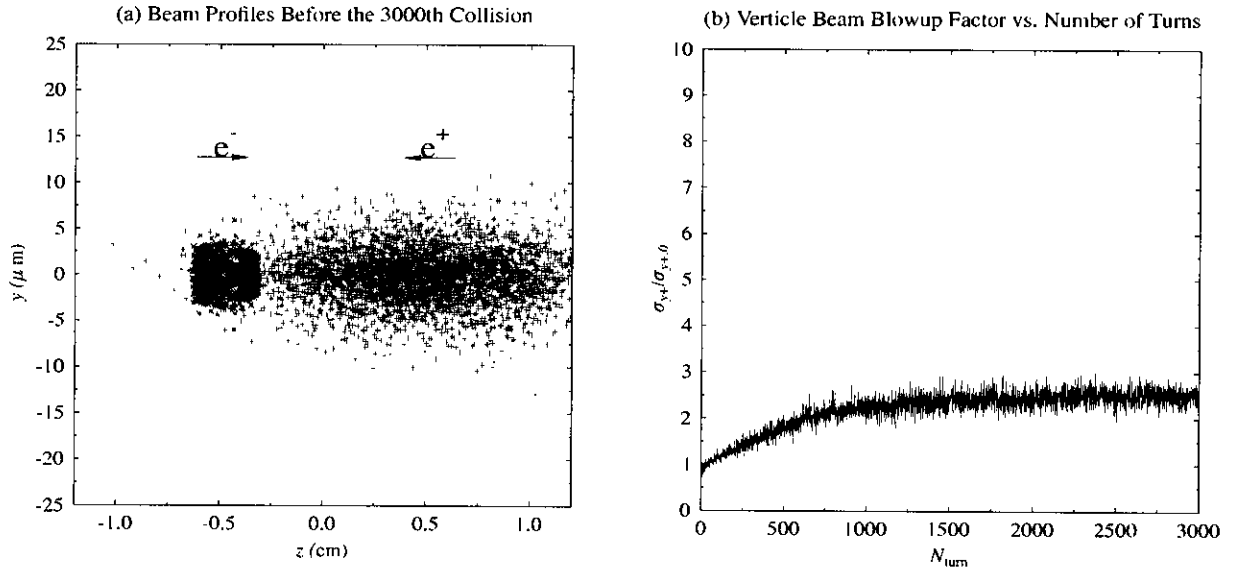


Figure 4: Simulation results using the number of macro-particles $N_{m-} = 1440$ for the electron bunch and $N_{m+} = 4000$ for the positron bunch.

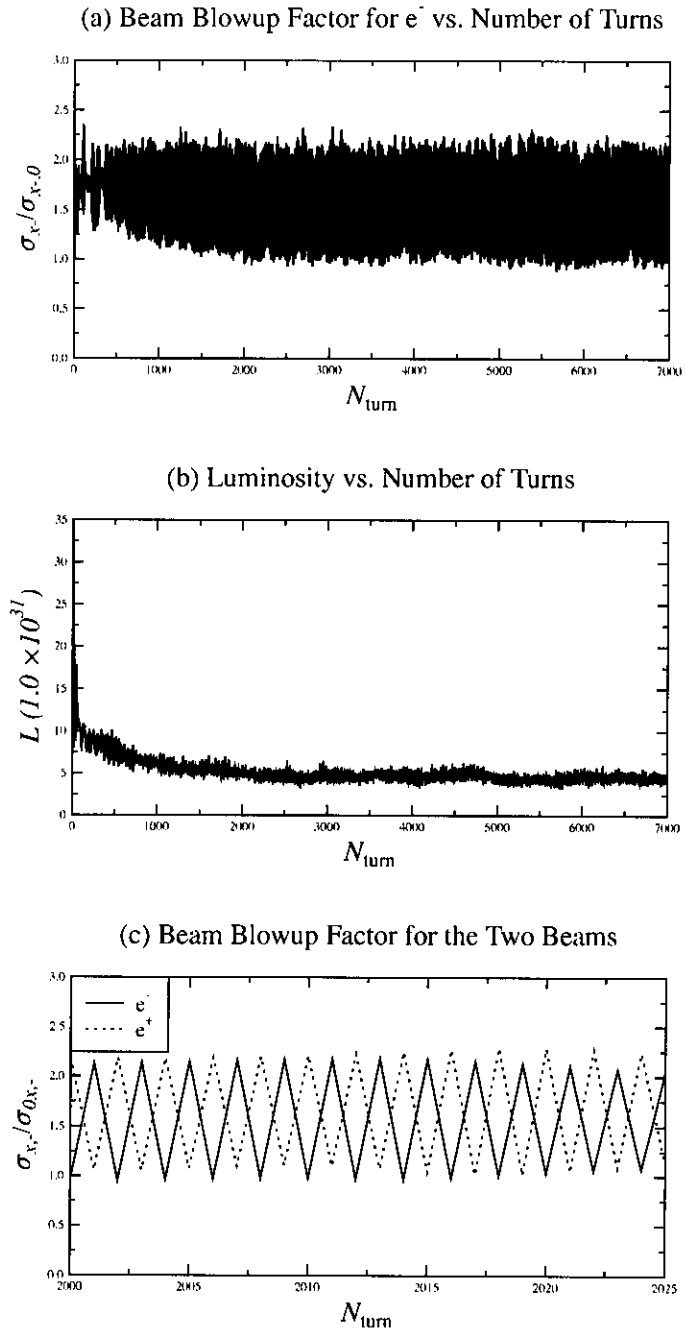


Figure 5: Coherent quadrupole resonance in ring/ring B factory for parameters in Table 1.

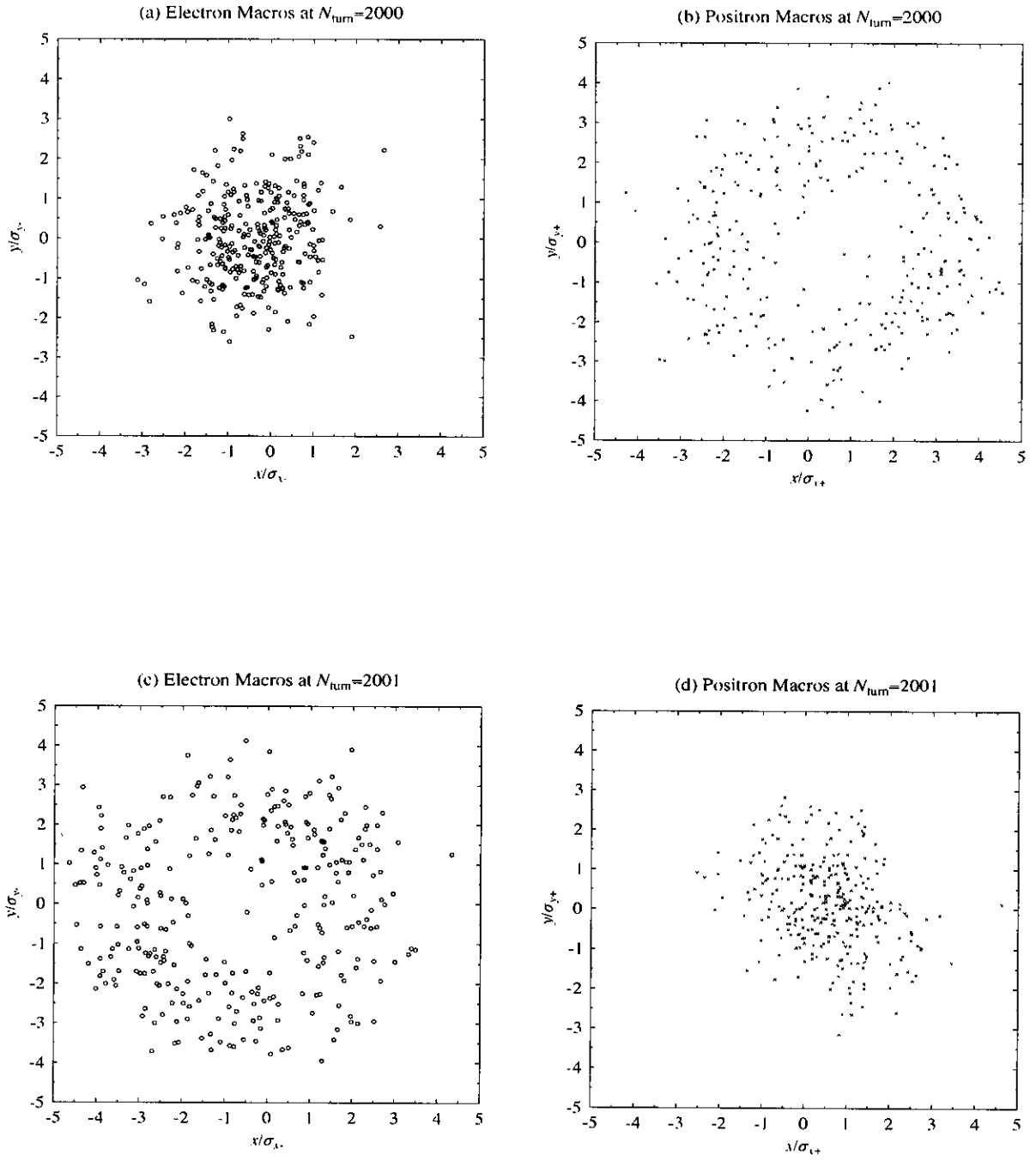


Figure 6: Transverse distribution of electron and positron bunches.

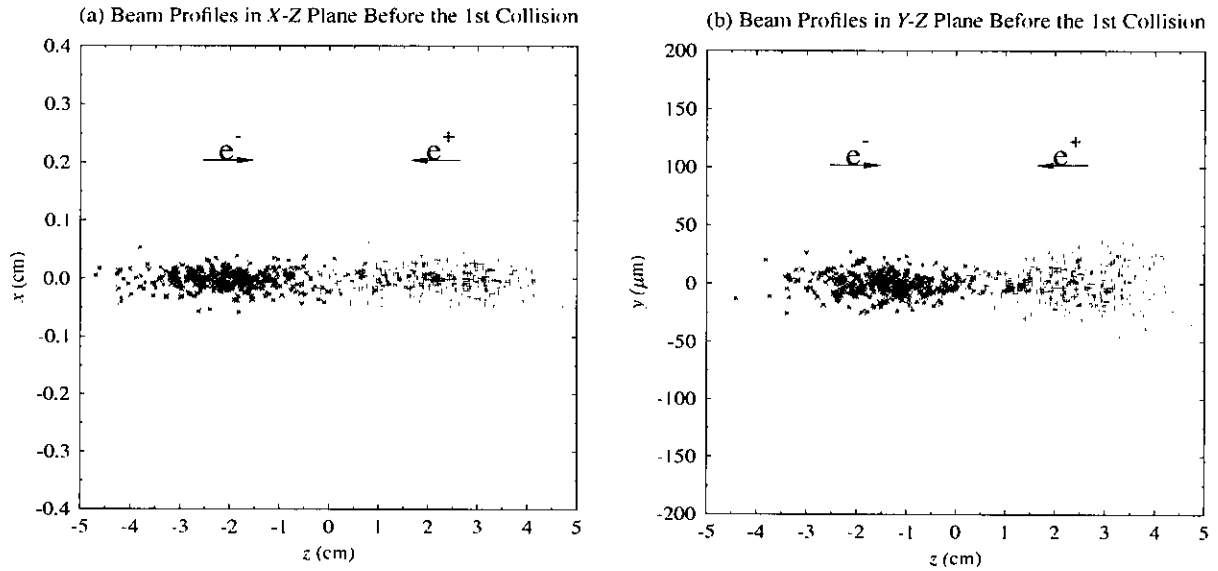


Figure 7: Initial beam profiles for beam-beam interaction in ring/ring collider using parameters in Ref. [7]

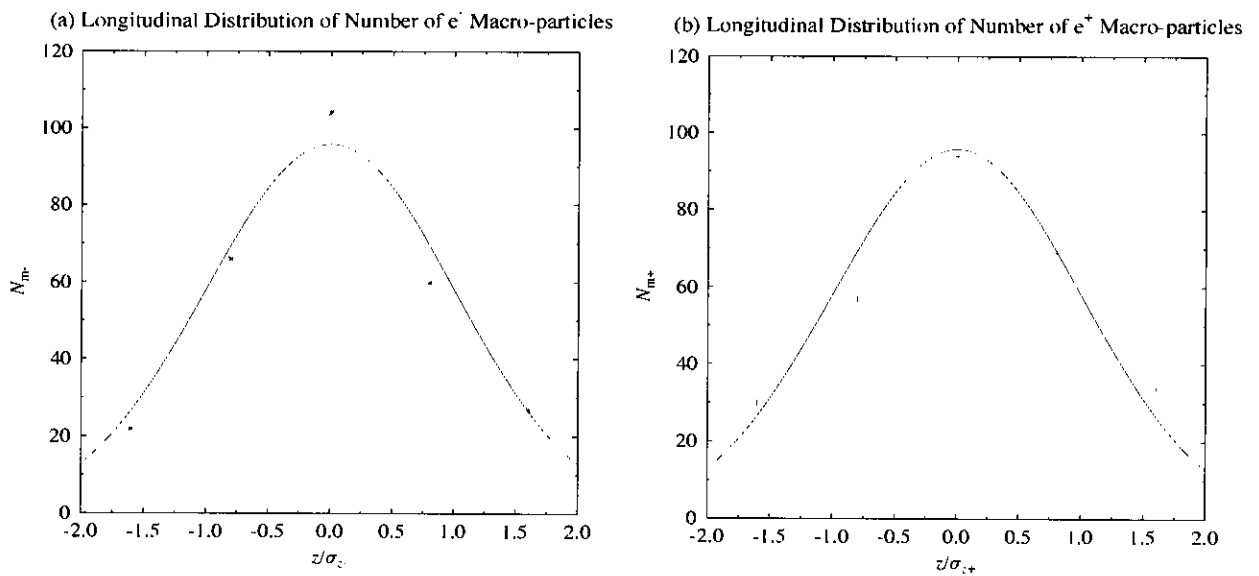


Figure 8: Initial numbers of macro-particles for the 5 slices in e^- and e^+ bunches respectively, which are compared with the ideal Gaussian distribution (solid curves).

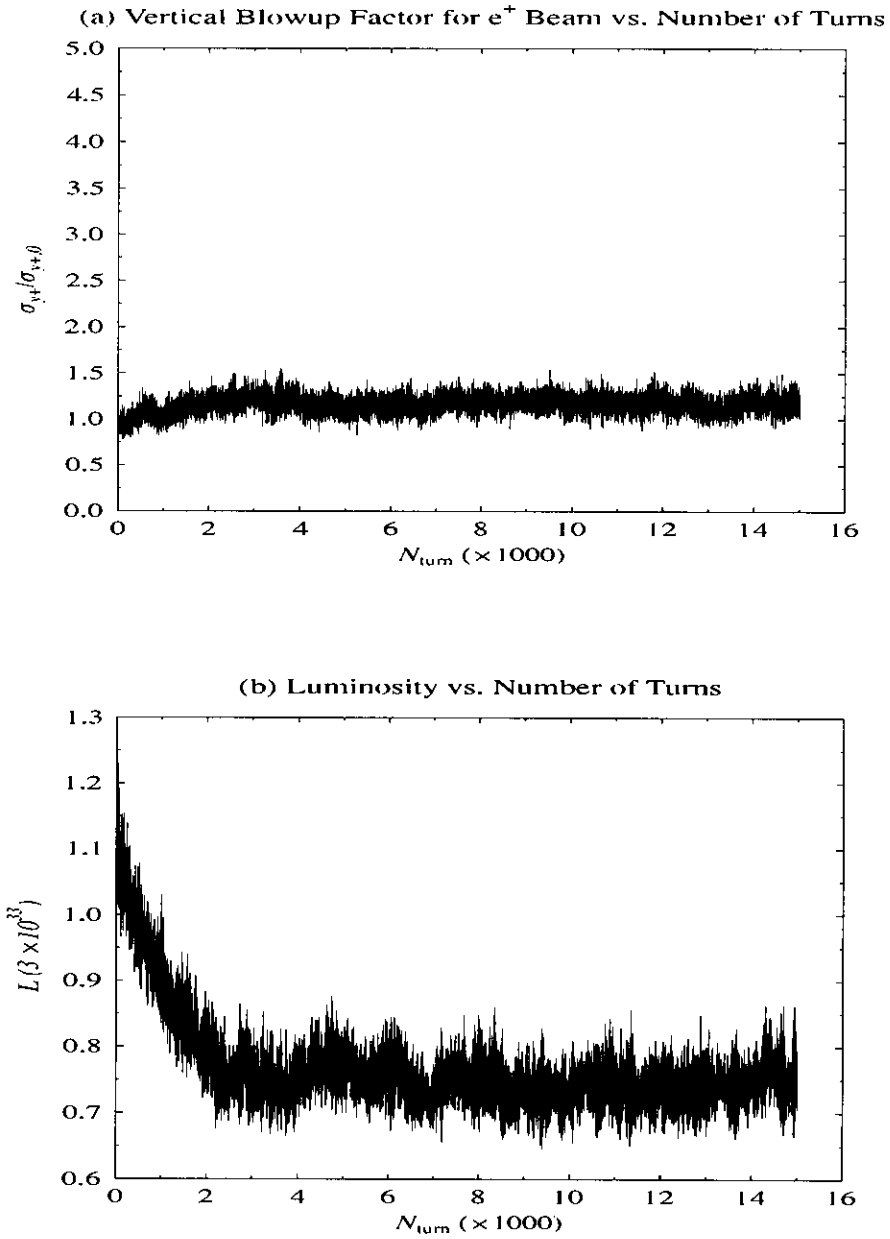


Figure 9: Results of (a) beam blowup for the positron beam and (b) luminosity during 15000 turns for parameters in Table 2.

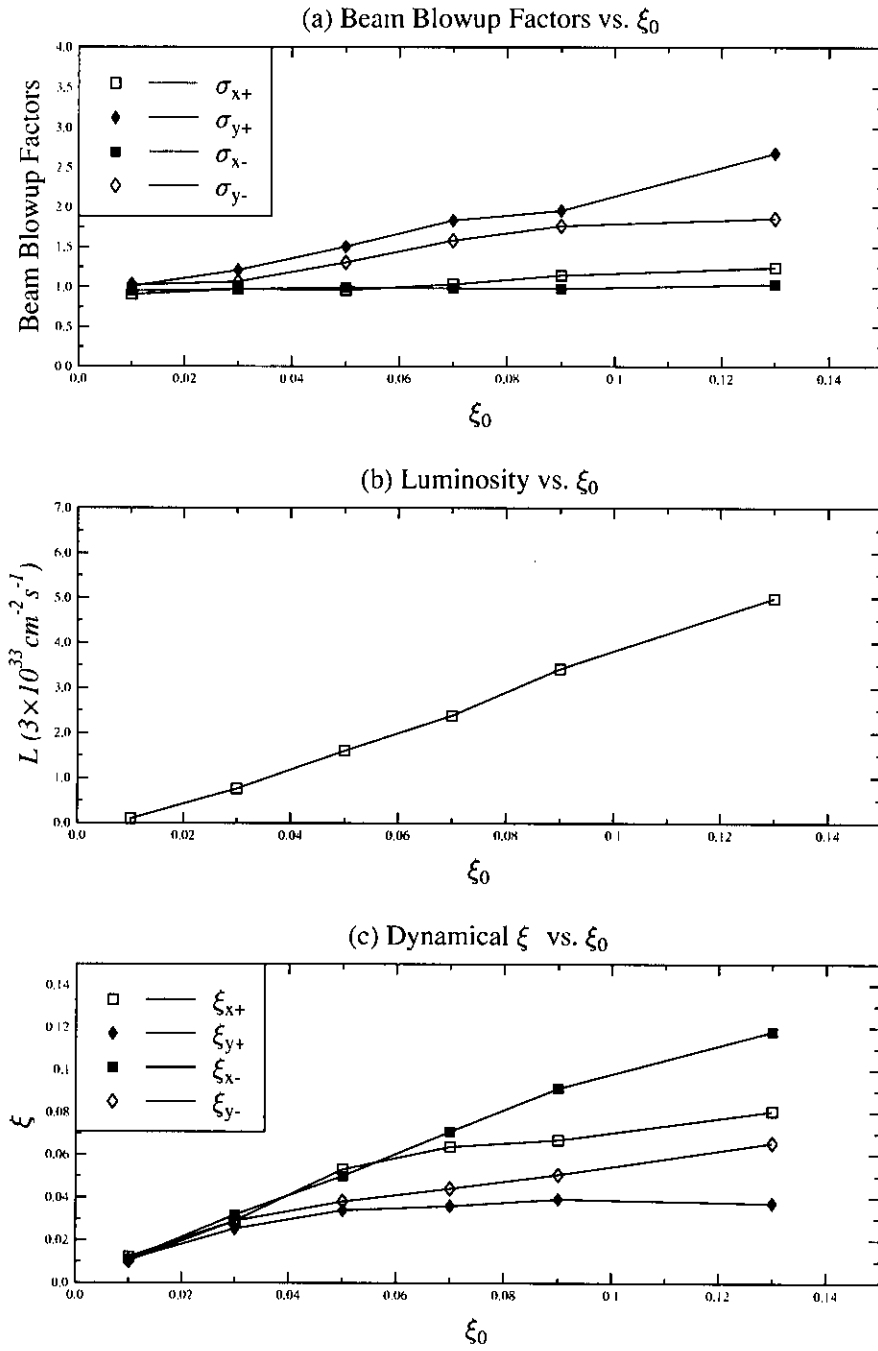


Figure 10: Results of beam-beam effect for ring/ring B Factory parameters.

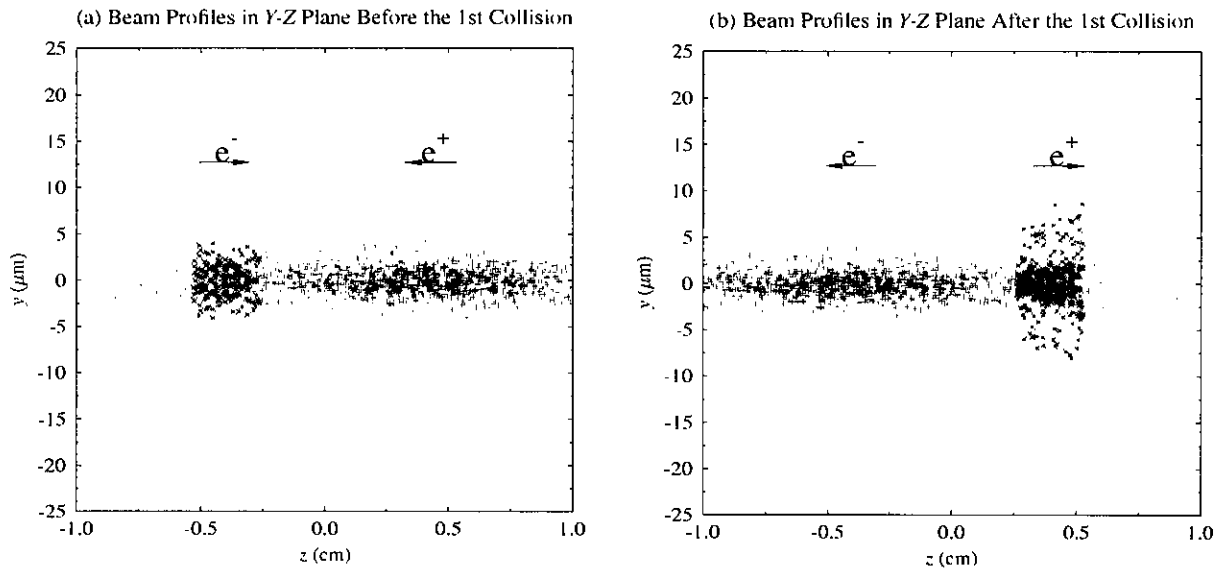


Figure 11: Beam profiles before and after the first collision with beam parameters shown in Table 3.

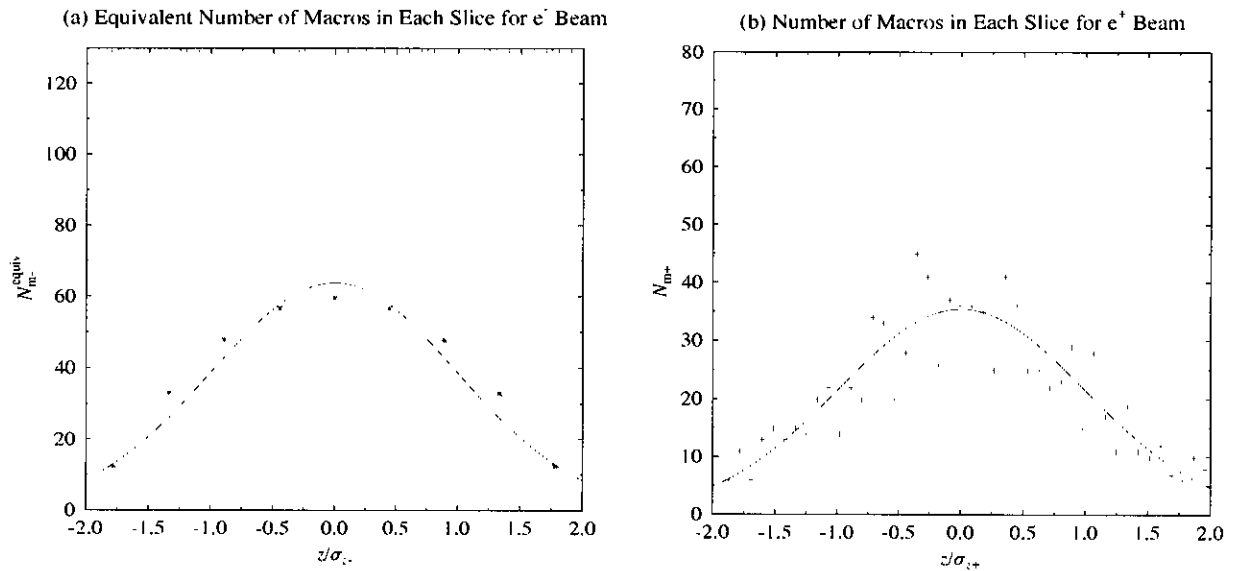


Figure 12: Longitudinal distribution of macro-particles in (a) e^- bunch and (b) e^+ bunch.

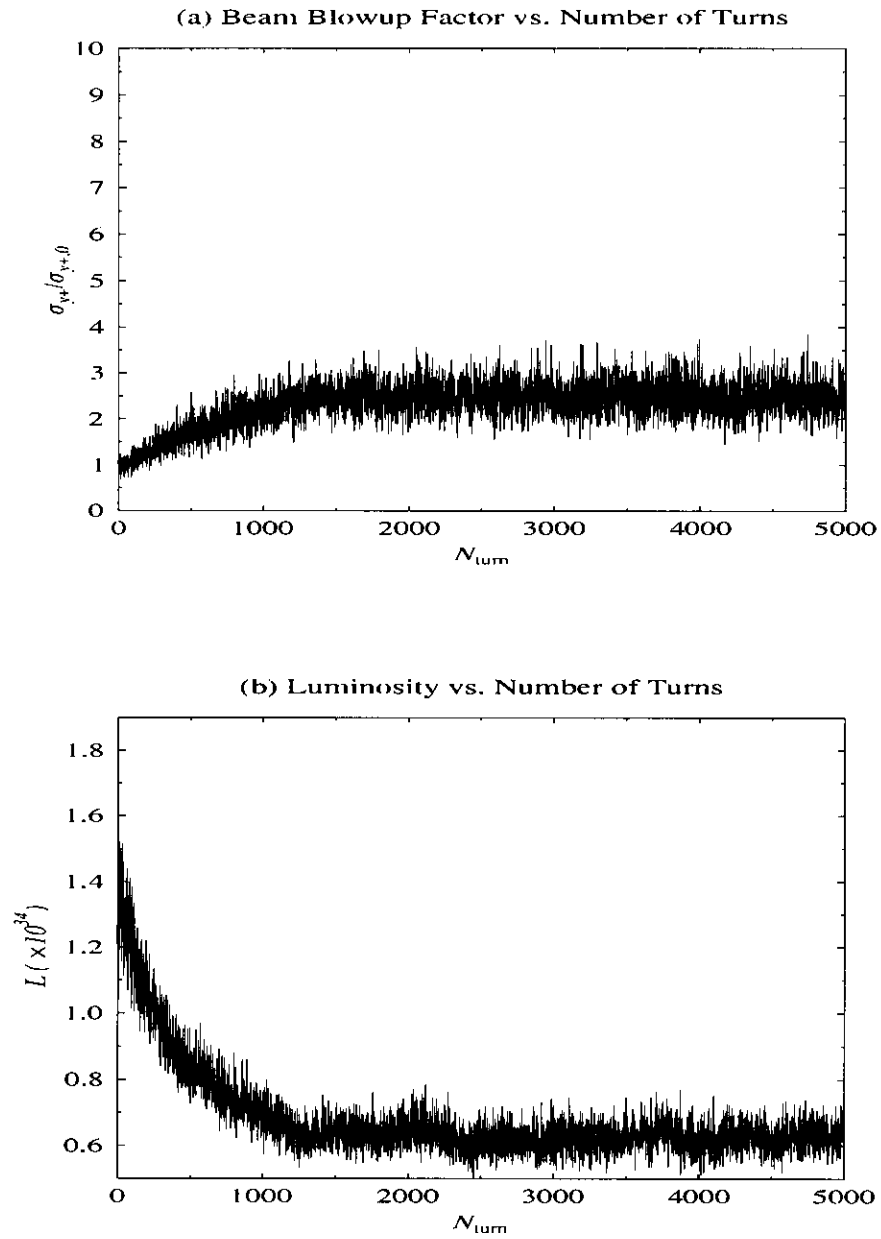


Figure 13: Results of (a) beam blowup for the positron beam and (b) luminosity during 5000 turns for parameters in Table 3.

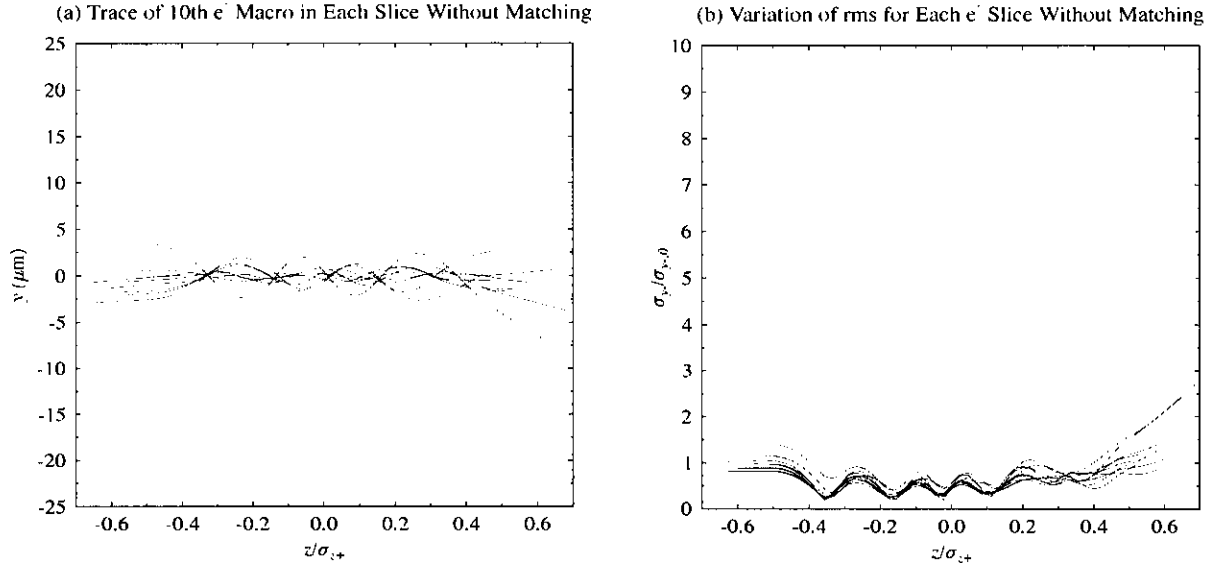


Figure 14: Plots of (a) traces of e^+ macros and (b) variations of rms for e^- slices in $Y - Z$ plane in the rest frame of the e^+ bunch *without* matching.

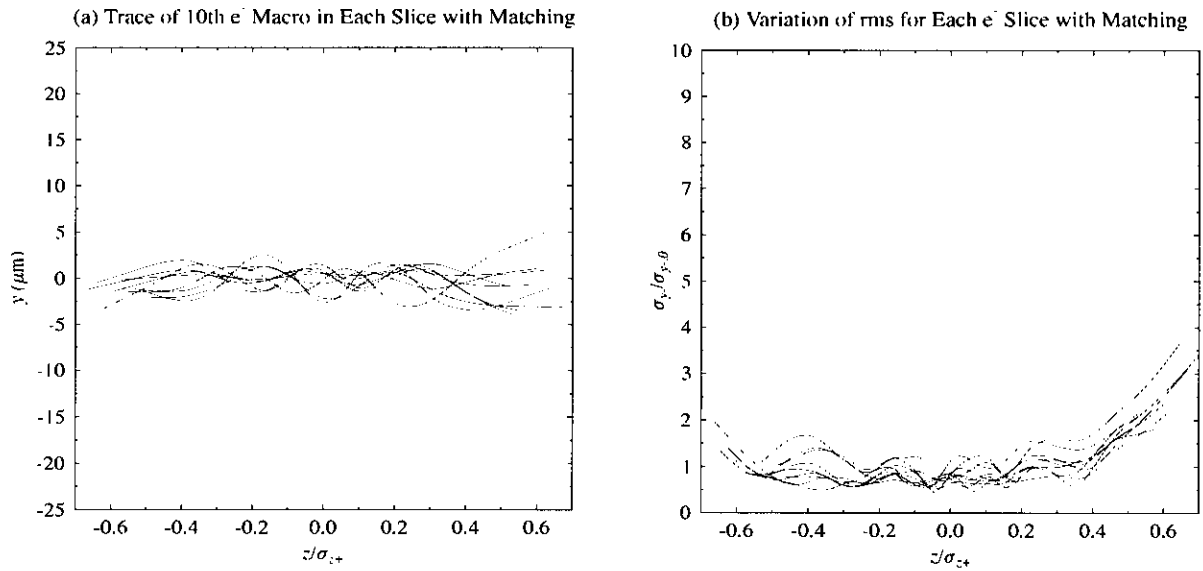
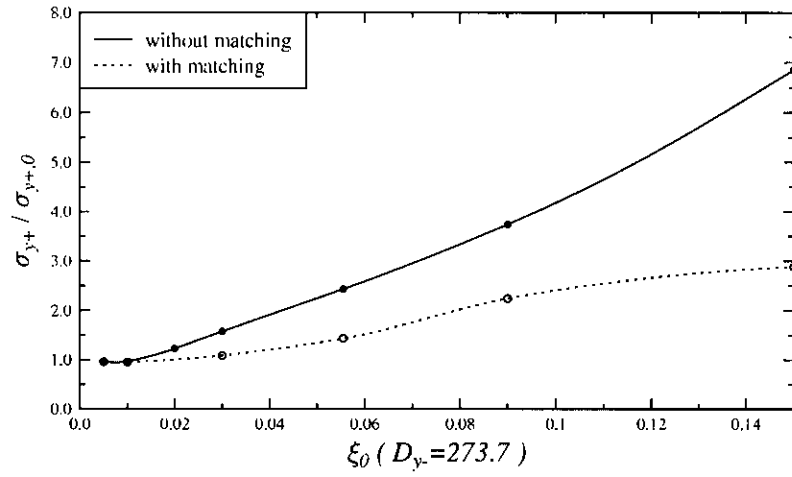


Figure 15: Plots of (a) traces of e^+ macros and (b) variations of rms for e^- slices in $Y - Z$ plane in the rest frame of the e^+ bunch *with* matching.

(a) Beam Blowup Factor vs. Nominal Tune Shift



(b) Luminosity vs. Nominal Tune Shift

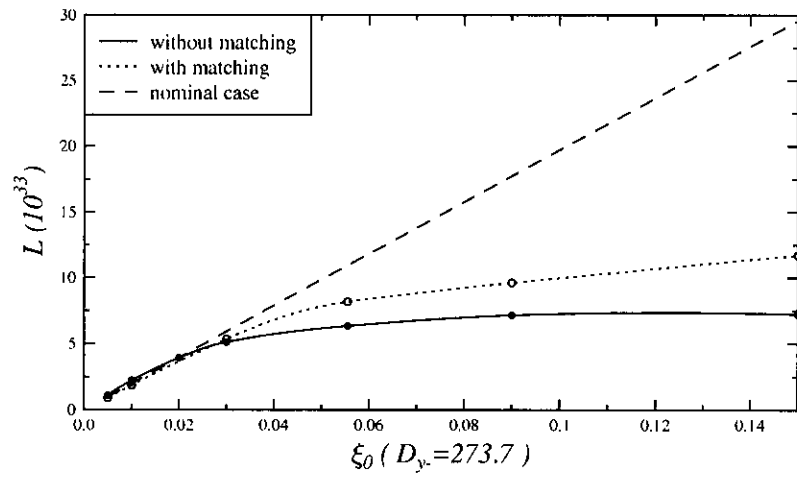


Figure 16: Results of beam-beam effect for a linac/ring B Factory using parameters in Table 3. Here ξ_0 is changed by varying N_- only.

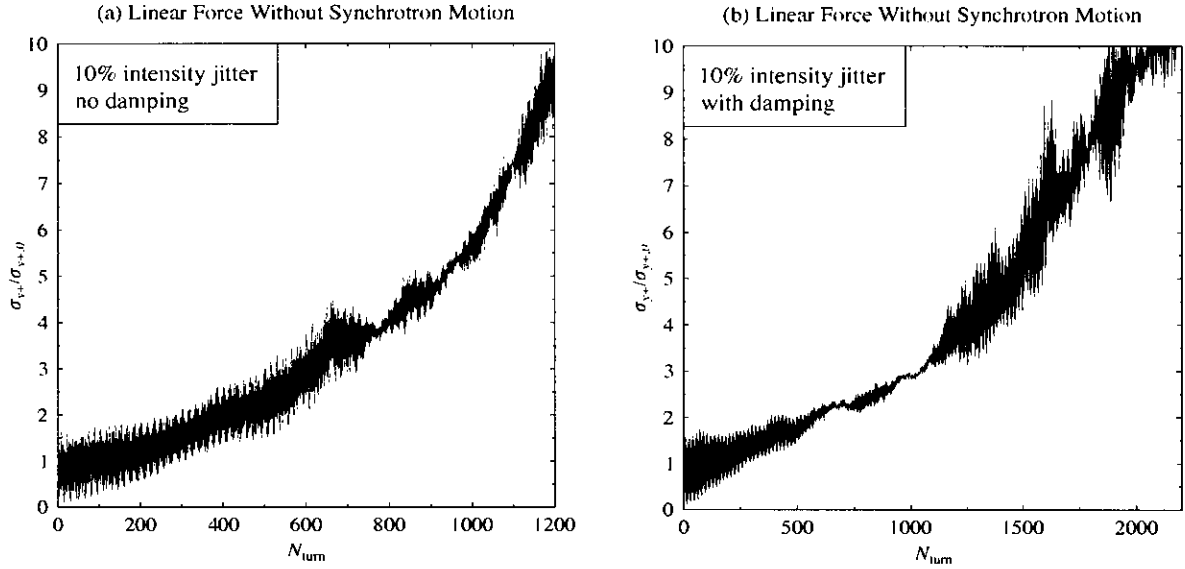


Figure 17: Vertical beam blowup for a round e^+ beam simulated by 500 particles. Here the analytic *linear* beam-beam transverse forces with $\xi_{x+,0} = \xi_{y+,0} = 0.055$ are used at IP for weak-strong simulation. The beam is assumed to have no longitudinal length.

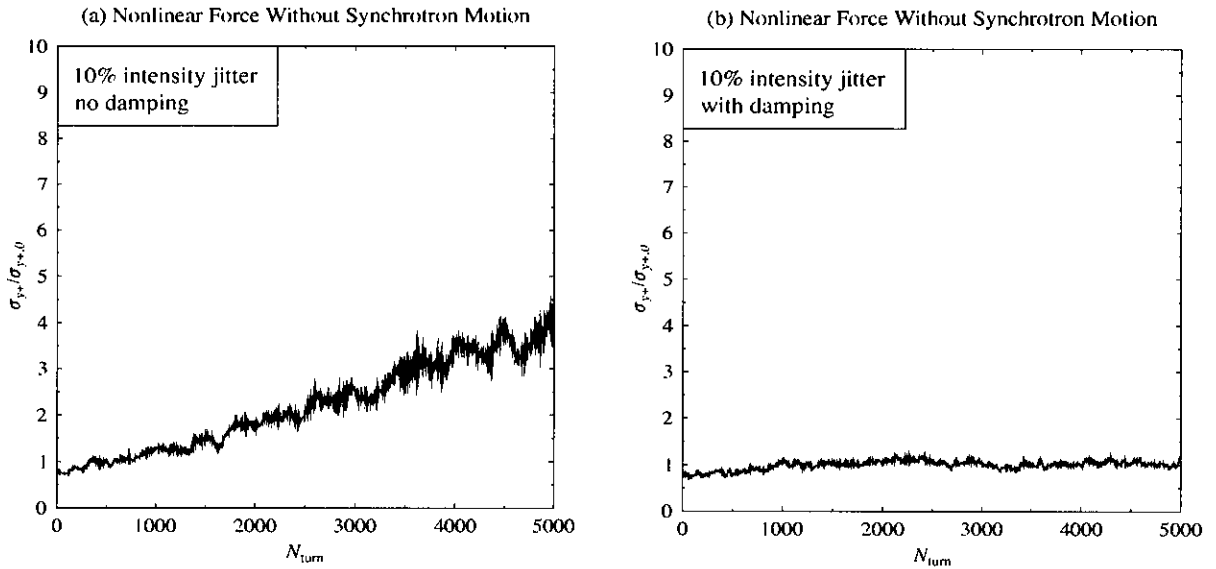


Figure 18: Vertical beam blowup for a round e^+ beam simulated by 500 particles. Here the analytic *nonlinear* beam-beam transverse forces with $\xi_{x+,0} = \xi_{y+,0} = 0.055$ are used at IP for weak-strong simulation. The beam is assumed to have no longitudinal length.

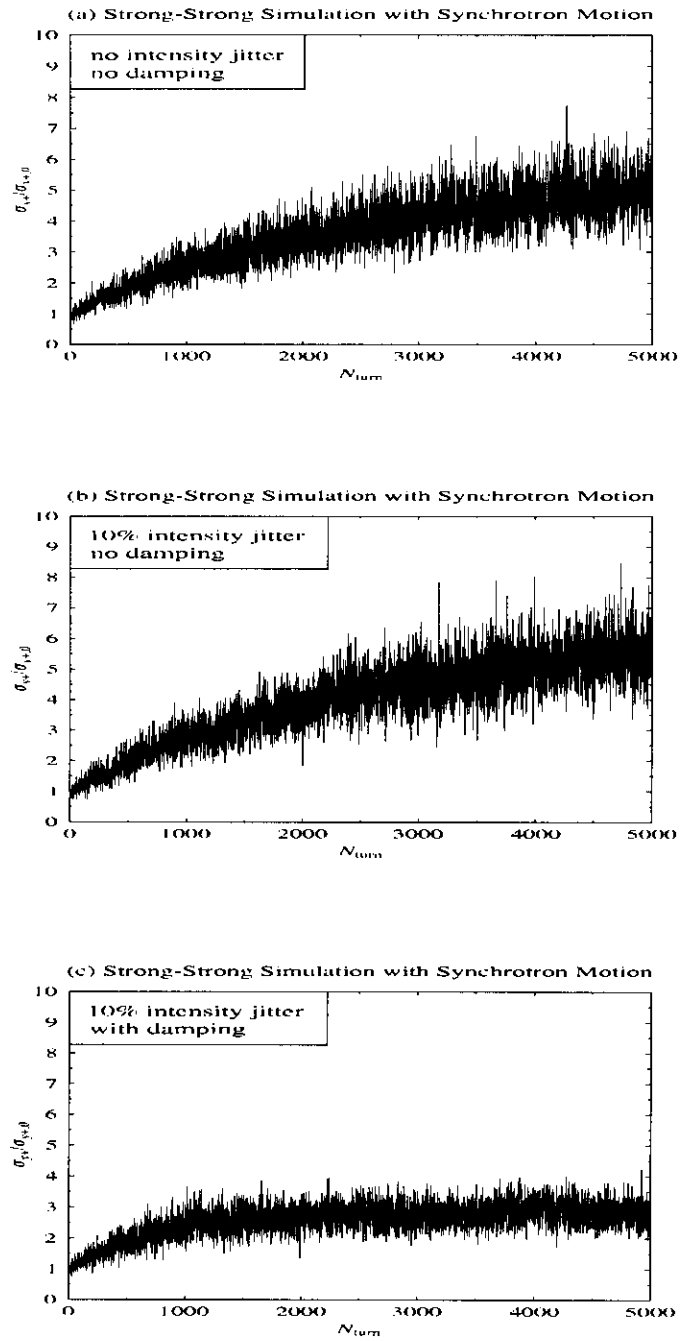


Figure 19: Vertical beam blowup in the strong-strong simulation, with parameters in Table 3.